Journal of Non-Crystalline Solids 619 (2023) 122554

Contents lists available at ScienceDirect

Journal of Non-Crystalline Solids

journal homepage: www.elsevier.com/locate/jnoncrysol

Deciphering the structural origins of high sulfur solubility in vanadium-containing borosilicate glasses

Rajan Saini [a,b], Daniel R. Neuville [c], Randall E. Youngman [d], Ashutosh Goel [a,*]

[a] Department of Materials Science and Engineering, Rutgers, The State University of New Jersey, Piscataway, NJ 08854-8065, United States
[b] Department of Physics, Akal University, Talwandi Sabo, Punjab 151302, India
[c] Institut de Physique du Globe de Paris, CNRS-Géomatériaux, Université de Paris, 1 rue Jussieu, 75005 Paris, France
[d] Science and Technology Division, Corning Incorporated, Corning, NY 14831, United States

ARTICLE INFO

Keywords:
Borosilicate
Glass
Sulfur
Vanadium
Nuclear waste
Structure

ABSTRACT

The addition of V_2O_5 has been long known to increase the sulfur (as SO_4^{2-}) solubility in borosilicate glasses. However, the mechanism governing this effect is still unknown. Although several studies have been published in the past two decades attempting to decipher the structural origins of increasing sulfur solubility as a function of V_2O_5 in borosilicate glasses, most of these studies remain inconclusive. The work presented in this paper attempts to answer the question, "Why does V_2O_5 increase sulfur solubility in borosilicate glasses?" Accordingly, a series of melt-quenched glasses in the system [30 Na_2O – 5 Al_2O_3 – 15 B_2O_3 –50 SiO_2]$_{(100-x)}$ – xV_2O_5, where x varies between 0 – 9 mol.%, have been characterized for their short-to-intermediate range structure and the redox chemistry of vanadium using ^{11}B, ^{27}Al, ^{51}V MAS NMR, Raman, and XPS spectroscopy. The impact of V_2O_5 on sulfur solubility in glasses has been followed by ICP-OES. The addition of $\leq$ 5 mol.% V_2O_5 results in a linear increase in sulfur solubility in the investigated glass system. Based on the results, we hypothesize that adding vanadium to the glasses increases their network connectivity, but reduces the network rigidity by replacing stronger Si–O–Si linkages with weaker Si–O–V linkages and forming $(VO_3)_n$-single chains. These modifications to the glass structure increase the flexibility of the network, thus making it possible to accommodate SO_4^{2-} in their voids/open spaces.

1. Introduction

While scientists and engineers around the world are working towards developing efficient processes and glass chemistries to enhance the loading of nuclear wastes into borosilicate glasses, one major bottleneck impeding this effort is the low solubility of sulfur in these vitreous waste forms [1–7]. In general, sulfur (as sulfate, SO_4^{2-}, in nuclear waste) solubility in the nuclear waste borosilicate glasses is considered to be $\leq$ 1 wt.% [2-4,8-10]. Exceeding the solubility limit of sulfur in the glass melt would result in the precipitation of an immiscible salt layer (known as *"gall"* or yellow phase) containing a high concentration of alkali/alkaline-earth sulfates and certain radionuclides (e.g., Tc, Sr, and Cs). Once formed, the salt layer would float on top of the melt resulting in the corrosion of sidewalls of the melter and short-circuiting the heating electrodes [11–14]. Hence, the practical concentration of sulfur in the borosilicate waste form is intentionally kept much lower than its solubility limit, thus, reducing the overall waste loading of the waste form, thereby increasing the volume of the glass to be produced and the cost of the whole clean-up mission.

In order to avoid the aforementioned complications and design advanced glassy waste forms with enhanced waste loading, researchers have adopted a two-pronged approach. In the first approach, researchers are working towards developing empirical models to predict the practical limit of sulfur (batched as SO_3) solubility in the melt as a function of the feed composition [4,15]. Being empirical, this approach solely relies on the amount of data and the statistical models employed to predict the limits of sulfur solubility [4,16,17]. The higher the number of data points pertaining to sulfur solubility in borosilicate glasses designed over a broad composition space, the more reliable and accurate are the predictions. The current machine learning-based models developed to predict sulfur solubility in nuclear waste glasses are based on 1074 glass compositions and exhibit an accuracy of R = 0.83, where R is the Pearson correlation coefficient and mean absolute percentage error (MAPE) of 42.99% [17]. Although this model does a reasonable job in

* Corresponding author.
E-mail address: ag1179@soe.rutgers.edu (A. Goel).

https://doi.org/10.1016/j.jnoncrysol.2023.122554
Received 15 April 2023; Received in revised form 2 August 2023; Accepted 3 August 2023

predicting the sulfur solubility in the nuclear waste borosilicate glasses (primarily focused on Hanford low-activity waste and high-level waste chemistries), the low values of R and MAPE suggest significant room for improvement in these models, which will require thousands of additional experimental data points.

The second approach is more scientific and relies on establishing the composition – structure – sulfur solubility relationships in borosilicate glass matrices with an overarching goal of developing Quantitative Structure-Property Relationship (QSPR) based models to predict sulfur solubility in the final waste form. However, this approach requires a comprehensive understanding of the compositional and structural descriptors controlling the solubility of sulfur in the glassy waste forms. Although efforts have been made in this pursuit, they have primarily been limited to qualitative analysis, where the results are explained based on semi-empirical crystallo-chemical parameters, e.g., cation-oxygen binding energy, Dietzel field strength, bond strength, size and polarization of polyhedra, etc. [9,18] or the structural details deciphered from qualitative/semi-quantitative spectroscopic techniques, e.g., Raman spectroscopy [2,12,19]. These studies are immensely helpful in establishing the composition–structure–property relationships at a "qualitative level," and in simplified compositions, thus laying the foundation of our knowledge about this subject. Nonetheless, their implications in multicomponent complex nuclear waste glasses are limited to the cause–effect relationships.

More recently, state-of-the-art spectroscopic techniques, for example, magic angle spinning – nuclear magnetic resonance (MAS NMR) spectroscopy and neutron diffraction, combined with other qualitative/semi-quantitative techniques, for example, Raman spectroscopy, have been employed to determine the compositional and structural dependence of sulfur solubility in both simplified and complex borosilicate based nuclear waste glasses [10,20-23]. While we are slowly progressing towards realizing the development of QSPR models to predict sulfur solubility in nuclear waste glasses, there are still several arduous questions about the role of additives (e.g., V_2O_5) or components from the nuclear waste (e.g., Cr_2O_3, Fe_2O_3, Cl) in the structure of borosilicate glasses and their consequent effect on sulfur solubility in the final waste form that need to be answered before we can successfully accomplish this goal. One such question that needs to be addressed is, "why does V_2O_5 increase sulfur solubility in borosilicate glasses?"

In the late-1980s, Russian researchers suggested that incorporating V_2O_5 in borosilicate glasses increases their sulfur solubility by enhancing the liquid state miscibility of sulfates in the glass melt [18]. Based on the crystallo-chemical parameters, it was proposed that the cations in a glassy matrix could be arranged into increasing order of sulfur solubility as [18]:

$$S_{IV}^{6+} - P_{IV}^{5+} - V_{IV}^{5+} - B_{III}^{3+} - Si_{IV}^{4+} - B_{IV}^{3+} - Al_{IV}^{3+} - Zn_{IV}^{2+}$$

where subscripts represent the cation coordination; according to this series, the closer the cation is to the SO_4^{2-} anion, the higher the sulfur solubility. For example, sulfate tetrahedra share better compatibility with phosphate tetrahedra than silicate ones, which explains the higher sulfate solubility within the phosphate matrices. Further, because the vitreous V_2O_5 primarily comprises $V^{5+}O_4$ tetrahedra with a structure similar to the PO_4 tetrahedra, i.e., V═O apex bond with three bridging oxygens, in addition to a minor fraction of VO_5 pyramids (later experimentally shown by McKeown et al. [24]), it has been assumed that V_2O_5 additions to borosilicate glasses will enhance their sulfur solubility. Although their assumption is correct, as V_2O_5 addition to the borosilicate glasses has been shown to increase their sulfur solubility [2,25], the reason behind their assumption, i.e., the similarity between the structures of $V^{5+}O_4$ and $P^{5+}O_4$, is most likely incorrect due to the following reasons: (1) their assumption is based on high sulfur solubility in glassy phosphate matrix, which is chemically and structurally different from the borosilicate glassy matrix; (2) P_2O_5, when added to a borosilicate glass, tends to induce phase separation in the glassy matrix [26]; (3) our preliminary (unpublished) results exhibit a negative impact of P_2O_5 on sulfur solubility in borosilicate glasses; (4) no other research group could reproduce the high sulfur loadings (up to 10 wt.% SO_3) in borosilicate glasses published by the Russian researchers [2].

Nevertheless, the positive impact of V_2O_5 on sulfur solubility in borosilicate glasses enticed researchers to unearth the mechanism governing this effect. In this pursuit, McKeown et al. [24] employed X-ray absorption spectroscopy to investigate the coordination and local environments of vanadium and sulfur in simulated borosilicate-based nuclear waste glasses. However, they did not find any evidence of V–S bonds or vanadium bonding to sulfate tetrahedra, even in the glasses with the highest concentration of V_2O_5, i.e., 11.85 wt.%. Later, Manara et al. [2] and Sengupta et al. [27] also attempted to reveal this mechanism by employing Raman and ^{11}B, ^{29}Si MAS NMR spectroscopy, respectively. However, they could not conclusively answer this long-standing question and recommended further detailed investigations.

Based on our understanding of the composition–structure–sulfur (as SO_3) solubility relationships, the following are the four chemo-structural drivers that primarily control the sulfur incorporation in borosilicate glasses: (1) degree of polymerization of the glass network; (2) availability of network modifying alkali/alkaline-earth cations to charge-compensate the SO_4^{2-} tetrahedra; (3) ionic field strength of non-framework cations; and (4) the redox behavior of multivalent ions in the melt, e.g., $V^{3+}O_4$, $V^{4+}O_5$, $V^{5+}O_4$[24,25,28]. The present study attempts to answer the question "why does V_2O_5 increase sulfur solubility in borosilicate glasses?" by considering all the aforementioned chemo-structural drivers (except ionic field strength because the glass compositions do not include multiple alkali/alkaline-earth cations). Accordingly, a suite of state-of-the-art spectroscopic techniques, including ^{11}B, ^{27}Al, and ^{51}V MAS NMR, Raman, X-ray photoelectron spectroscopy (XPS), and inductively coupled plasma–optical emission spectroscopy (ICP-OES) have been employed to study the structure, vanadium redox chemistry and sulfur solubility in a series of melt-quenched glasses in the system (30 Na_2O – 5 Al_2O_3 – 15 B_2O_3 – 50 SiO_2)$_{(100-x)}$ – $(V_2O_5)_x$, where x varies from 1 to 10 mol.%. Finally, an attempt has been made to correlate the structural descriptors of glasses with their sulfur solubility and decode the reason for the positive impact of vanadium on sulfur solubility.

2. Experimental details

2.1. Synthesis of sulfur-free glasses

The V_2O_5-free baseline glass chosen for this study, with composition 30 Na_2O – 5 Al_2O_3 – 15 B_2O_3 – 50 SiO_2 (mol.%), is the simplified version of ORPLG27 LAW glass [20], where Na_2O represents the combination of all the alkali and alkaline-earth oxides. The glasses were synthesized by the melt quench technique. High purity powders of SiO_2 (Alfa Aesar; >99.5%), H_3BO_3 (Alfa Aesar; >98%), and Na_2CO_3 (Fisher Scientific; >99.5%) were used as precursors. NH_4VO_3 (Alfa Aesar; > 99%) was used as a precursor to incorporate V_2O_5 in the glass. For each glass composition, batch calculations were made for 70 g glass. Before melting the glass, the calculated amount of NH_4VO_3 was mixed with SiO_2 and Al_2O_3 and calcined at 500 °C for 2 h to volatilize ammonia from the batch. The calcined mixture was homogenously mixed with an appropriate amount of H_3BO_3 and Na_2CO_3 and melted in 90%Pt –10%Rh crucibles (loosely covered with a Pt lid) in an electric furnace at 1200 °C for 1 h. The melt was quenched on a copper plate maintained at room temperature.

2.2. Synthesis of sulfur-containing glasses

Na_2SO_4 has been used as a precursor for incorporating sulfur in glasses. The batch calculations were made to ensure that the total content of Na_2O in the glass remains constant. The example below describes the methodology used to synthesize sulfur-containing glasses in the present study. When adding x mol.% SO_3 to a sulfur-free composition,

for example, 35 Na_2O – 5 Al_2O_3 – 10 B_2O_3 – 50 SiO_2, the batch was calculated as (35-*x*) Na_2O – 5 Al_2O_3 – 10 B_2O_3 – 50 SiO_2 – *x* Na_2SO_4 (mol. %), where *x* mol.% Na_2SO_4 serves as the source of *x* mol.% Na_2O and *x* mol.% SO_3. Accordingly, a batch corresponding to composition (35-*x*) Na_2O – 5 Al_2O_3 – 10 B_2O_3 – 50 SiO_2 was prepared and melted in a Pt-Rh crucible using the methodology described in Section 2.1. Once the melt (poured on the copper plate) cooled to room temperature, the resulting glass was returned to the same Pt–Rh crucible and *x* mol.% Na_2SO_4 was added to it. The Pt–Rh crucible was loaded in the furnace and covered with a Pt lid. The mixture was melted at the same temperature (as the sulfur-free glass) for another hour, followed by quenching of the melt by pouring it on a copper plate kept at room temperature.

2.3. Compositional analysis of glasses

The amorphous/crystalline nature of the resulting samples has been confirmed by powder (particle size < 45 μm) X-ray diffraction (PANalytical X'Pert Pro-X-ray diffractometer with Cu K_α radiation; 45 kV; 40 mA; 2θ range of 10 - 90°; step-size of 0.013°; dwell time of 0.01 s at each step). The compositional analysis of the glass samples has been performed by ICP–OES (Perkin Elmer Optima 8300). The methodology to prepare the samples for the ICP-OES analysis has been described in our previous article [10]. Table 1 presents the batched and analyzed compositions (as obtained using ICP-OES) of the baseline, sulfur-free (but vanadium-containing), and sulfur-containing glasses investigated in the present study. The sulfur-free glasses are labeled as *x*V, where *x* represents the molar concentration of V_2O_5 in the glass. Similarly, the sulfur-containing glasses are labeled as *x*V-*y*S, where *y* represents the molar concentration of SO_3 (batched) in the glass.

2.4. Structural analysis of glasses

^{11}B and ^{27}Al MAS-NMR spectra of the glasses have been acquired using a commercial spectrometer (VNMRs, Agilent) and a 3.2 mm MAS NMR probe (Agilent). The samples were powdered in an agate mortar, packed into 3.2 mm zirconia rotors, and spun at 22 kHz for ^{27}Al, and 20 kHz for ^{11}B MAS NMR. ^{27}Al MAS NMR data have been collected at 16.4 T (182.33 MHz resonance frequency) with a 0.6 μs (~π/12 tip angle) pulse width for uniform excitation of the resonances, recycle delays of 2 s and averaging of 1000 acquisitions. ^{11}B MAS NMR experiments have been conducted at 16.4 T (224.52 MHz resonance frequency), incorporating a 4 s recycle delay, short radiofrequency (rf) pulses (0.6 μs) corresponding to a π/12 tip angle, and signal averaging of 400 to 1000 scans. Fitting of the MAS NMR spectra has been performed using DMFit [35]. The CzSimple model, which accounts for distributions in the quadrupolar coupling constant, has been utilized for ^{27}Al MAS NMR spectra. For ^{11}B MAS NMR data, "Q MAS 1/2″ and Gaus/Lor functions have been used to fit 3- & 4-fold coordinated boron resonances, respectively, accurately reproducing the 2nd-order quadrupolar line shapes of 3-fold coordinated boron. A minor correction for the 4-fold coordinated boron peak has been applied due to its overlapping satellite transition [36].

^{51}V MAS NMR data have been collected using an Agilent DD2 spectrometer, Agilent 5 mm MAS NMR probe, and at an external field strength of 4.7 T, corresponding to a ^{51}V resonance frequency of 52.51 MHz. The glass samples were powdered with an agate mortar/pestle and loaded into 5 mm zirconia rotors. The sample spinning was performed with compressed nitrogen and computer controlled to 10.0 kHz. 1000 acquisitions were co-added using a rf pulse width of 0.8 μs (~ π/10 tip angle) and a 2 s recycle delay. The data were processed with commercial software, and the shift reference was determined using the International Union of Pure and Applied Chemistry (IUPAC) method of ratioing the shift of ^{51}V relative to that measured with another nucleus (i.e., ^{13}C in adamantane) [29]. NMR parameters, quadrupolar coupling constant (C_Q), and isotropic chemical shift were estimated using the CzSimple lineshape model in DMFit.

Unpolarized Raman spectra were collected at room temperature over 300 to 1600 cm^{-1} with a precision of ±5 cm^{-1}, using an HR Horiba spectrometer. The excitation source was the 488 nm line of a solid state laser operating at 200 mW. The measurements were performed at different positions on the sample surface to ascertain sample homogeneity.

The XPS measurements were performed on freshly fractured monolithic vanadium-containing glass samples to analyze and quantify the oxidation states of vanadium in the investigated glasses. The XPS measurements utilized Thermo Scientific K-Alpha equipment, which used a 1486.6 eV monochromatic Al Kα x-ray source to excite core-level electrons from the sample. A low-energy dual electron/argon-ion beam flood gun was used for charge compensation during measurements. The kinetic energy of the photoelectrons was measured using a 180° double-focusing hemispherical analyzer with a 128-channel detector. Binding energies were referenced to the main component of the adventitious carbon peak at 284.8 eV. The photoelectron spectrometer was calibrated using the $Au4f_{7/2}$ binding energy (83.96 eV) for the etched surface of the Au metal reference. The analyzer was operated in constant resolution mode with a pass energy of 10 eV for high-resolution spectroscopy, while a pass energy of 50 eV was used for the routine survey scans. Peak fitting for the core-level scans was performed using a mixed Gaussian-Lorentzian function (Gaussian: 85%) to obtain binding energy and FWHM of the peaks. Peak areas were converted to composition using suitable elemental relative sensitivity factors [30] and corrected for attenuation through an adventitious carbonaceous overlayer using a calculation similar to the method described by Smith [31].

2.5. Density and thermal analysis

The density measurements have been performed on the monolithic glass samples using the Archimedes principle. A hydrostatic balance with D–limonene (specific gravity at 25 °C = 0.84 g/cc) as the immersion fluid has been used to measure the submerged weight of the glasses. The density data reported for any glass composition is an average of at least nine measurements (3 pieces of glass; each piece measured thrice) with a standard deviation of <0.0014 g/cc. Molar volume (V_m) of glasses

Table 1
Batched and experimentally measured (within ±0.2 wt.%) glass compositions (in parentheses) of *x*V and *x*V-*y*S glasses. The reported SO_3 concentration for any composition corresponds to its solubility limit in that glass.

Glass ID *x*V	Na_2O (wt.%)	B_2O_3 (wt.%)	SiO_2 (wt.%)	Al_2O_3 (wt.%)	V_2O_5 (wt.%)	SO_3 (wt.%)
0V	28.97 (28.95)	16.27 (16.26)	46.81 (46.82)	7.94 (7.94)	0	0
1V	28.16 (28.14)	15.82 (15.83)	45.51 (45.52)	7.72 (7.73)	2.78 (2.77)	0
2.5V	27.00 (27.01)	15.17 (15.16)	43.62 (43.61)	7.40 (7.40)	6.77 (6.76)	0
5V	25.21 (25.20)	14.16 (14.16)	40.74 (40.73)	6.91 (6.92)	12.98 (12.98)	0
7.5V	23.56 (23.57)	13.23 (13.24)	38.07 (38.06)	6.46 (6.46)	18.68 (18.67)	0
9V	22.63 (22.64)	12.71 (12.71)	36.56 (36.56)	6.20 (6.20)	21.89 (21.88)	0
Glass ID *x*V-*y*S	Na_2O (wt.%)	B_2O_3 (wt.%)	SiO_2 (wt.%)	Al_2O_3 (wt.%)	V_2O_5 (wt.%)	SO_3 (wt.%)
1V-1.25S	26.89 (26.87)	15.76 (15.77)	45.35 (45.36)	7.70 (7.71)	2.77 (2.78)	1.53 (1.51)
2.5V-1.75S	25.27 (25.25)	15.10 (15.11)	43.44 (43.45)	7.37 (7.38)	6.74 (6.75)	2.08 (2.06)
5V-3S	22.38 (22.37)	14.05 (14.06)	40.42 (40.42)	6.86 (6.86)	12.88 (12.89)	3.40 (3.39)
7.5V-6S	18.19 (18.17)	13.04 (13.05)	37.51 (37.52)	6.36 (6.37)	18.41 (18.41)	6.48 (6.47)
9V-6.5S	16.97 (16.95)	12.51 (12.51)	36.00 (36.01)	6.11 (6.12)	21.55 (21.53)	6.81 (6.83)

has been calculated using the equation:

$$V_m = \frac{M_w}{\rho} \quad (1)$$

where M_W and ρ represent the molecular weight and density of the glass, respectively.

The differential scanning calorimetric (DSC) scans have been obtained on the glass samples to determine the onset of glass transition temperature (T_g). The DSC measurements have been performed using a simultaneous thermal analyzer, STA-449F Jupiter, manufactured by Netzsch, Germany. The glass samples were crushed and sieved to a particle size range of 0.85 mm to 1 mm. The measurements were performed in Pt–Rh (10 wt.% Rh) pans covered with a Pt–lid. The samples were heated from 100 to 1000 °C at 10 °C/min in air. An empty Pt–Rh pan was used as a reference. The reported data for each glass is an average value of at least three scans.

3. Results

3.1. Redox chemistry of vanadium in the investigated glasses

The images of vanadium-containing aluminoborosilicate glasses are shown in Fig. 1. The color of the glass changes from yellow to dark brown as the concentration of V_2O_5 increases from 1 mol.% to 9 mol.%, thus suggesting +5 as the dominant oxidation state of vanadium in the glass structure [32]. Further increase in the V_2O_5 concentration to 10 mol.% results in a visible phase separation/crystallization, while the glass shows a mix of blue and dark brown colors. Here it should be noted that the blue color is a characteristic of tetravalent vanadium [32,33].

All *x*V glasses have been found to be XRD amorphous, as shown in Fig. 2a. Although the XRD analysis shows the 10 V sample to be amorphous, the presence of traces of crystallinity in this glass are confirmed by optical microscopy (Fig. 2b). Therefore, this glass composition has not been investigated further. Also, based on the studies reported by Sengupta et al. [27] and Halder et al. [34], the possibility of phase separation in the glasses with $V_2O_5 > 5$ mol.% was considered. Accordingly, the mirror-polished (unetched) glass samples from compositions 7.5 V and 9 V were observed under a scanning electron microscope (SEM) equipped with energy dispersive spectroscopy (EDS). However, no phase separation was observed in the investigated glasses (images not shown). Further investigations using transmission electron microscopy (TEM) may be required to confirm the presence/absence of nano-scale phase separation in these glasses, if any. Nonetheless, for the present study, the investigated glasses have been considered to be homogeneous.

Fig. 1. Images of V_2O_5-containing sulfur-free glasses (*x*V); glasses *x*V-*y*S where sulfur solubility limit has been reached; and glasses *x*V-*y*S supersaturated with sulfur showing the formation of salt layer on their surface.

According to the literature [32,35], the color of a V_2O_5-containing glass depends on the atmosphere during melting and the alkali (alkaline-earth)–to–aluminum ratio in the glass composition. Replacing Na^+ with Li^+ or K^+ does not significantly affect the color of vanadium-containing glasses [32]. However, moving from per-alkaline to per-aluminous regimes has been shown to change the color of glass from yellow to brown [35], both being characteristic colors of vanadium in +5 oxidation state [32]. According to Weyl [32], the pentavalent vanadium forms yellow-to-brown colored oxide which resemble chromic acid (CrO_3), but due to its acidic nature, it usually forms a colorless metavanadate (VO_3^-) anion in the solutions. Similarly, while a V_2O_5-containing soda lime silica glass melted under ambient conditions is yellow, the re-melting of the same glass under reducing conditions has been shown to change its color to emerald green, thus indicating the presence of V^{3+} as the dominant species [32]. According to Cicconi et al. [35] the V_2O_5-free aluminosilicate glasses exhibit the UV-edges below 300 nm wavelength in their optical absorption spectra and are, therefore, colorless. However, the glasses doped with a low concentration of V_2O_5 (up to 2.5 mol.% in the present study) are supposed to have their UV edges in the visible region around 400 nm, absorbing the violet light and giving the characteristic yellowish color. Further, in the glasses with higher V_2O_5 content (>2.5 mol.%), the shoulders of the UV-edge at 500 nm tend to cut the contributions from blue light, thus, leading to more brownish colors.

The qualitative analysis of the redox chemistry of vanadium (based on their physical appearance) in the investigated *x*V glasses is further corroborated by their XPS analysis. Fig. 3a presents the XPS spectra of the O 1 s and V 2p core levels from each sample. The untreated spectra are shown using dots for each data point, whereas the solid lines are the same spectra after applying a 10-point (1.0 eV) smoothing spline. Each spectrum exhibits the following four distinct features: (1) Na KL2 Auger emission line (537 eV); (2) O 1 s core level (531 eV); (3) V $2p_{3/2}$ (517 eV); and (4) V $2p_{1/2}$ (524 eV) core level states. An accurate deconvolution of the V 2p envelope is complicated (if not impossible) due to its relatively low signal-to-noise ratio and an additional unknown peak that overlaps with the V $2p_{1/2}$. Therefore, to semi-quantitatively determine the oxidation state of vanadium in the glasses as a function of V_2O_5 content, the binding energy at the maximum height of the smoothed data has been calculated and plotted in Fig. 3b. In glasses with V_2O_5 <7.5 mol.%, the binding energy of the V $2p_{3/2}$ peak is around 517.3 eV, which is near the expected binding energy of 517.91 eV for the V^{5+} oxidation state [36]. At higher concentrations (≥7.5 mol.% V_2O_5), the V $2p_{3/2}$ peak shifts to a lower binding energy, suggesting the presence of V^{4+} species, whose peak is expected to be at 516.35 [36]. Thus, the XPS analysis suggests that vanadium exists primarily in +5 oxidation state in the investigated glasses. The presence of vanadium in +4 oxidation state in glasses with $V_2O_5 \leq 5$ mol.%, although cannot be negated, is minimal. In glasses with higher V_2O_5 content (>5 mol.%), a notable fraction of V^{4+}species is present.

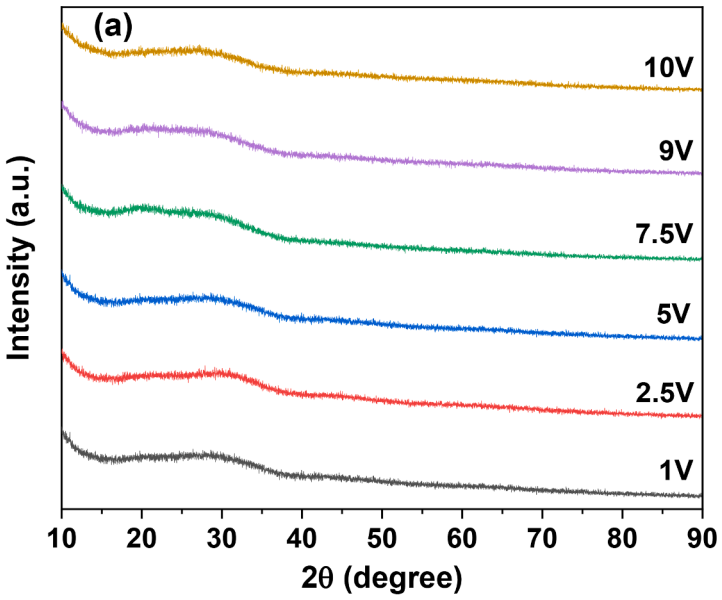

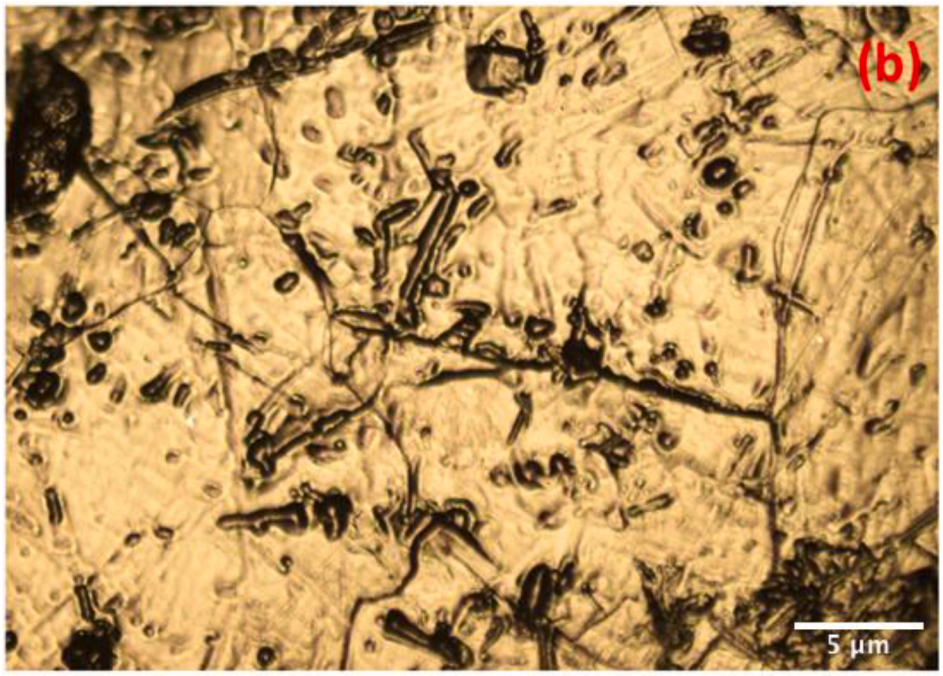

Fig. 2. X-ray diffractograms of (a) *x*V glasses and (b) optical microscope image of 10 V glass.

3.2. Impact of vanadium on the structure of glasses

3.2.1. Raman spectroscopy

Raman spectra of *x*V (baseline) glasses are shown in Fig. 4. In the low-frequency region (300–800 cm^{-1}), the Raman spectrum of baseline glass exhibits a broad envelope with characteristic bands around 520, 575, 632, and 747 cm^{-1}, respectively. The bands around 520 cm^{-1} and 575 cm^{-1} can be attributed to the mixed vibrations of T–O–T (T represents Si and Al tetrahedra) linkages and reedmergnerite-like borosilicate units [37,38]. The characteristic bands at 632 cm^{-1} and 747 cm^{-1} correspond to the danburite and pentaborate units in the glass network [37]. The mid-frequency region (800–1250 cm^{-1}) belongs to the stretching vibrations of TO_4 units and encompasses contributions from Q^n_{mAl} units, where n (= 0–4) is the number of bridging oxygens associated with silicate unit, and m (= 0–4) is the number of AlO_4 units in the next-nearest sphere of Si. Since the peak corresponding to this band is centered at ~1070 cm^{-1}, it is safe to assume that the Q^3 units form the backbone of the silicate network in the baseline glass [37]. The high-frequency region (1350–1600 cm^{-1}) is associated with stretching vibrations of metaborate ($B–O^-$) units linked to other BO_3 and BO_4 units in the glass network [37,39-41].

The addition of 2.5 mol.% V_2O_5 to the baseline alkali aluminoborosilicate glass leads to the appearance of two bands: a band at ~372 cm^{-1} corresponding to O–V–O vibrations [2], and a second band in the spectral region between 800 and 1000 cm^{-1} with its intensity maximum at 863 cm^{-1}, suggesting vanadium to primarily exist as $V^{5+}O_4$ units in the glass structure [24,35]. The addition of 5 mol.% V_2O_5 to the glass leads to two changes: (1) broadening of the ~863 cm^{-1} band along with a shift in its peak position from 863 cm^{-1} to 869 cm^{-1}; (2) appearance of a new peak at 913 cm^{-1}, which is associated with the vibration of $V^{4+}O_5$

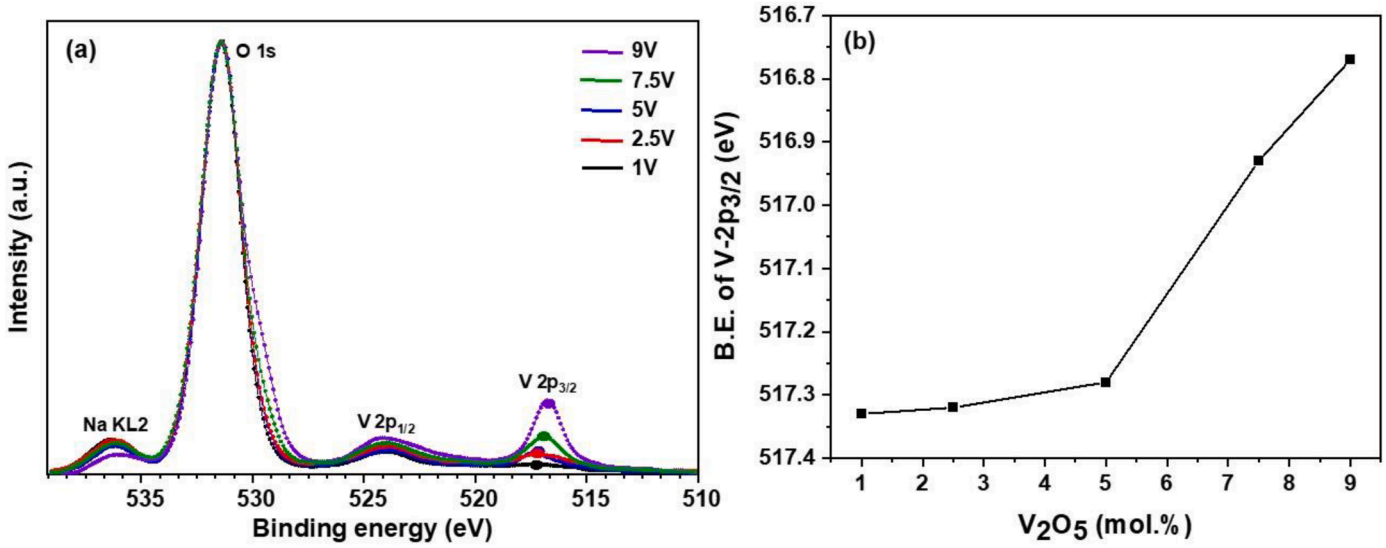

Fig. 3. (a) XPS spectra of the O 1 s and V 2p core levels of the *x*V glasses. The untreated spectra are shown using dots for each data point, whereas the solid lines are the same spectra after applying a 10 point (1.0 eV) smoothing spline. (b) Variation in the binding energy of V-$2p_{3/2}$ (at the maximum height of the smoothed data shown by circles in Fig. 3a) as a function of V_2O_5 concentration in the glasses.

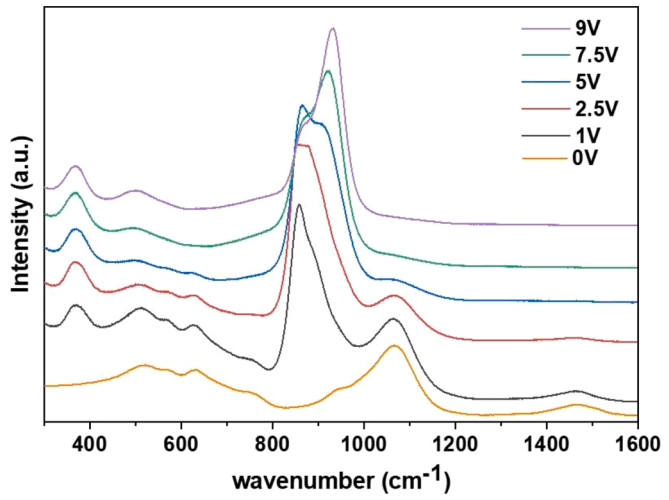

Fig. 4. Raman spectra of *x*V glasses along with 0 V glass.

units in the glass [2,42]. Further addition of V_2O_5 (>5 mol.%) leads to a decrease in the intensity of 869 cm^{-1} band along with a shift in the 913 cm^{-1} peak to ~937 cm^{-1}. These spectral features indicate a partial reduction of V^{5+} to $V^{4+}$and a change in the coordination environment of vanadium in the glass network.

With respect to the impact of V_2O_5 on the degree of polymerization in the silicate network, the addition of 1 mol.% V_2O_5 divides the 800 cm^{-1} – 1200 cm^{-1} band into two parts: (1) 800 cm^{-1} – 1000 cm^{-1} and (2) 1000 cm^{-1} to 1200 cm^{-1}. As discussed above, the 800 – 1000 cm^{-1} region is completely masked by VO_x bands. Therefore, it is difficult to decipher any changes in the fraction of Q^n (n = 1, 2) units in the glass structure as a function of V_2O_5 concentration. The band in the region 1000 cm^{-1} to 1200 cm^{-1} is centered at ~1070 cm^{-1}, confirming the presence of Q^3 and Q^4 units, where Q^3 units are in the majority. An increase in the V_2O_5 concentration, from 1 mol.% to 5 mol.%, results in a gradual decrease in the intensity of the 1000 cm^{-1} to 1200 cm^{-1} band, leading to its complete disappearance in glasses with 7.5 mol.% and 9 mol.% V_2O_5. The complete disappearance of the Raman band comprising Q^3 and Q^4 units suggests either a significant degree of depolymerization induced by V_2O_5 in the silicate network, wherein the aluminosilicate network most likely comprises Q^n (n = 0, 1 and 2) units, or the replacement of stronger Si–O–Si linkages by weaker Si–O–V linkages, thus, shifting the band to lower wavenumbers. Since the molar volume of the glasses is increasing with an increase in V_2O_5 content (discussed in Section 3.2.3), suggesting an increase in directional bonding in the glass structure [43,44], the latter scenario seems more plausible. The structural results are in good agreement with the dissolution studies on the investigated glasses (unpublished results), where it has been observed that adding V_2O_5 (up to 5 mol.%) to the baseline glass increases its dissolution kinetics in Tris–HCl solution and deionized water in part due to a decrease in Si–O–Si linkages.

3.2.2. *^{11}B, ^{27}Al and ^{51}V MAS NMR spectroscopy*

Fig. 5a depicts the ^{27}Al MAS NMR spectra of *x*V glasses with a broad peak centered around 60 ppm assigned to the tetrahedrally-coordinated AlO_4 units (hereafter referred to as A^{IV}) in the glass structure [45,46]. Weaker resonances are also apparent upon close inspection, including a small amount of five-coordinated Al (Al^V) under the upfield portion of the asymmetric Al^{IV} peak and a small feature around 0 ppm from Al in the zirconia rotors (i.e., background signal) [47]. Quantitative details of Al speciation and related NMR parameters have been obtained by fitting the ^{27}Al MAS NMR spectra, and the results are listed in Table 2. An increase in the V_2O_5 concentration does not significantly affect the aluminum coordination in the aluminoborosilicate glass network, as evident from the nearly identical spectra in Fig. 5a and an essentially constant fraction of Al^{IV} and Al^V groups. Nonetheless, adding V_2O_5 results in the systematic broadening of the Al^{IV} resonance, which likely arises from interactions between Al^{IV} groups and paramagnetic vanadium species [48]. Another change in the ^{27}Al MAS NMR spectra with increasing V_2O_5 is a progressive shift of the Al^{IV} resonance towards lower ppm values, suggesting a change in the next-nearest neighbor polyhedra around Al, similar to what has been observed in P_2O_5-containing aluminosilicate and aluminoborosilicate glasses [49,50].

Fig. 5b presents the ^{11}B MAS NMR spectra of *x*V glasses with a relatively broad and complex resonance in the interval 10–20 ppm, reflecting strong quadrupolar interactions for the ^{11}B nuclei of three-coordinated boron (B^{III}) sites. A relatively narrow peak around 0 ppm corresponds to four-coordinated boron (B^{IV}) sites [51,52]. The addition of V_2O_5 to the baseline glass has a rather subtle impact on boron speciation, as the relative peak intensities for both B^{III} and B^{IV} are seemingly unaffected. Nevertheless, a closer inspection reveals the

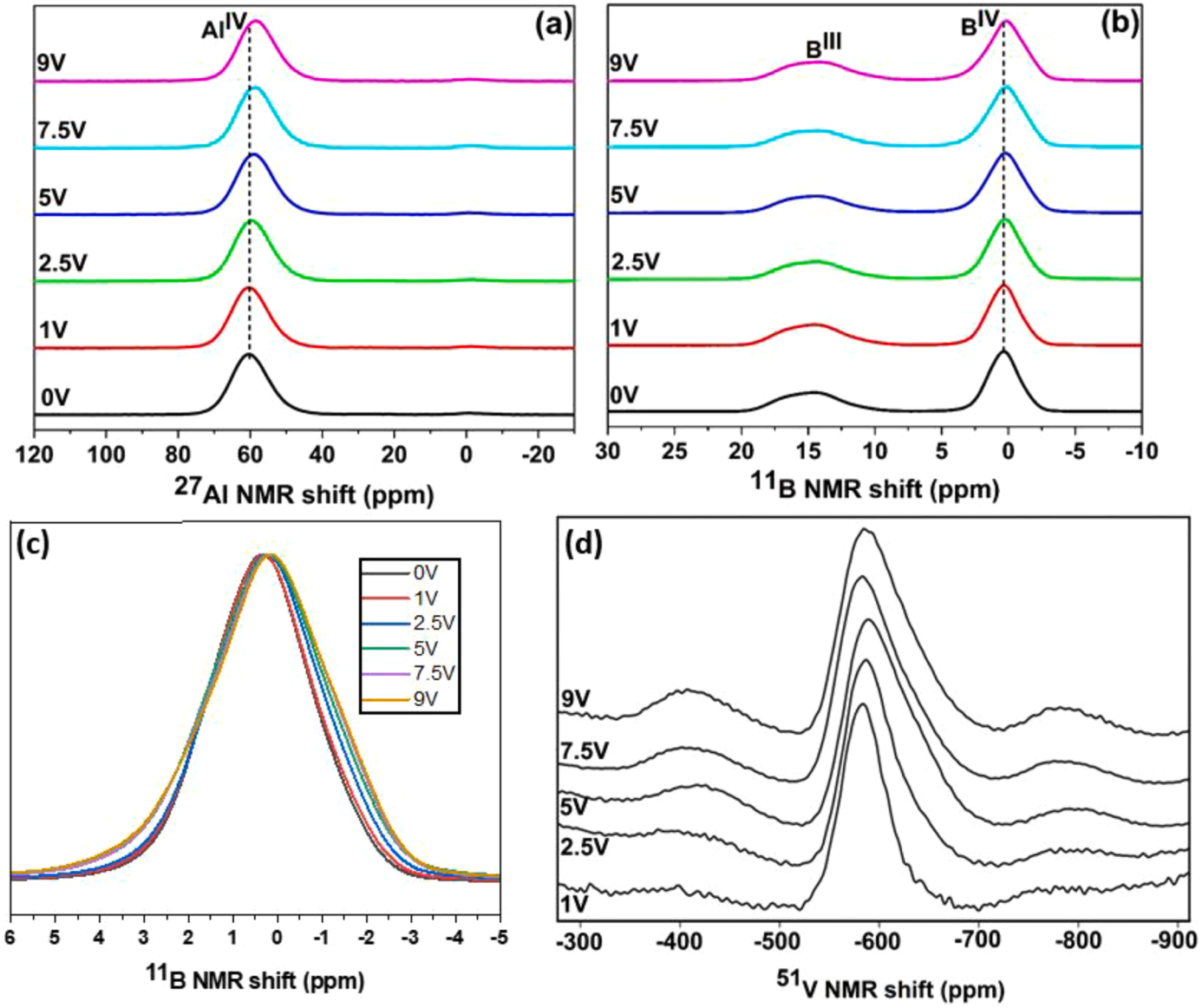

Fig. 5. (a) ^{27}Al, (b) ^{11}B, (c) shifting of B^{IV} peak position with V_2O_5 concentration, and (d) ^{51}V MAS NMR spectra of *x*V glasses.

Table 2
Results from the deconvolution of ^{27}Al MAS NMR spectra of *x*V glasses. The uncertainty in abundance, chemical shift (δ_{CS}) and quadrupolar coupling constant (C_Q) is ±1%, ±1 ppm and ±0.2 MHz, respectively.

Glass ID	Al^{IV}			Al^{V}		
	Atomic (%)	δ_{CS} (ppm)	C_Q (MHz)	Atomic (%)	δ_{CS} (ppm)	C_Q (MHz)
0V	97	63.8	4.39	3	32.7	3.24
1V	98	63.7	4.31	2	32.6	2.18
2.5V	98	63.0	4.35	2	32.9	2.21
5V	98	62.4	4.36	2	33.0	2.16
7.5V	98	62.1	4.38	2	33.1	2.14
9V	98	61.9	4.44	2	33.0	1.84

broadening and shifting of the B^{IV} peak towards lower ppm values (Fig. 5c), in line with the impact of V_2O_5 on the Al^{IV} NMR signal, as discussed above. We hypothesize that this may be attributed to the coupling between the boron nuclei and paramagnetic V^{4+} centers, as corroborated by an increase in the Lorentzian broadening of the B^{IV} NMR peak (centered at ~ 0.2 ppm) with an increase in V_2O_5 concentration and reduced V species (observed in the Raman/XPS analysis). Although there is a slight broadening in the trigonal B^{III} resonance peak, mainly for the 9 V glass, the observed change is much less obvious, which may indicate that VO_x polyhedra are more closely associated with the negatively charged AlO_4 and BO_4 groups than with neutral BO_3 units. The measured N_4 value ($= \frac{B^{IV}}{B^{III}+B^{IV}}$) for the 0 V glass is 59.3%, which gradually increases to 65.8% as V_2O_5 concentration increases up to 7.5 mol.%. As the V_2O_5 concentration is increased further (9 mol.%), the N_4 value decreases to 61.9% (Table 3). The observed trend pertaining to the variation in N_4 fraction as a function of V_2O_5 content in glasses is in good agreement with that predicted by Lu et al. [53] using molecular dynamic (MD) simulations and experimentally demonstrated by Muthupari et al. [54], and Saetova et al. [55] in alkali borovanadate glasses.

Fig. 5d presents the ^{51}V MAS NMR spectra of *x*V glasses with a symmetric resonance peak around −565 ppm (for 1 V, 2.5 V, and 5 V glass), which moves slightly towards more negative shift with increasing V_2O_5 – a trend observed in other vanadium-containing oxide glasses [48, 56]. The resonance peak exhibits a shift to −558 and −560 ppm for 7.5 V and 9 V glasses, respectively; however, the difference is small. The addition of V_2O_5 to the glass leads to a broadening of the central

Table 3
Fraction of borate species in the *x*V glasses estimated from the deconvolution of ^{11}B MAS NMR spectra, and the chemical shift (δ_{CS}) and quadrupolar coupling constant (C_Q) parameters obtained from ^{51}V MAS NMR spectra. The uncertainty in abundance, δ_{CS} and C_Q is ±1%, ±2 ppm and ±0.5 MHz, respectively.

Glass ID	Boron speciation		^{51}V	
	N_3 (%)	N_4 (%)	δ_{CS} (ppm)	C_Q (MHz)
0V	40.7	59.3	—	—
1V	41.8	58.2	−565	4.6
2.5V	36.8	63.2	−565	5.6
5V	35.4	64.6	−564	6.5
7.5V	34.2	65.8	−556	6.5
9V	38.1	61.9	−560	6.5

resonance peak and increases the intensity of additional sidebands arising from the paramagnetic interactions due to reduced V^{4+} species [48], as observed in the Raman and XPS analysis. The quadrupolar coupling constant (C_Q) increases from 4.6 to 6.5 MHz as V_2O_5 increases from 1 mol.% to 5 mol.% and remains ~ 6.5 MHz for higher V_2O_5 glasses (7.5 V and 9 V). Since the spectra are broad and likely affected by the paramagnetic spins associated with reduced V, it is unreliable to deconvolute them to get accurate information about the coordination environment of vanadium in the glass structure. The estimated chemical shifts and quadrupolar coupling constants are summarized in Table 3 and, in general, are similar to those reported in V-doped lithium silicate glasses [57] and crystalline alkali metavanadates [58].

3.2.3. Density, molar volume, and glass transition temperature

Fig. 6 presents the glass transition temperature (T_g) of the *x*V glasses as a function of V_2O_5 content. The T_g value of the baseline (0 V) glass is 485 °C. The T_g remains nearly constant (~486 °C) with the addition of 2.5 mol.% V_2O_5 to the baseline glass. However, it decreases to 462 °C with the addition of 5 mol.% V_2O_5. Further increase in the V_2O_5 concentration subtly affects the T_g of the glasses as it decreases to 454 °C for glasses containing 7.5 and 9.0 mol.% V_2O_5. The results agree with those reported in the literature [35,54] and can be explained based on the Adam – Gibbs model of glass transition [59]. The activation barriers for the structural rearrangement in melt may decrease when stronger silicate and borate linkages are substituted by weaker vanadate linkages, enlarging the liquidus regime. Hence, it results in lowering the T_g values.

The density (ρ) of the *x*V glasses increases from 2.45 g cm^{-3} to 2.49 g cm^{-3}, and the molar volume increases from 24.58 cm^3 mol^{-1} to 28.19 cm^3 mol^{-1} with the addition of V_2O_5 (1–9 mol.%), as shown in Fig. 7. The observed trends in the variation in density and molar volume are in agreement with the literature [60] and can be attributed to the (1) addition of an oxide with higher density (ρ_{V2O5} = 3.36 g cm^{-3}) and (2) expansion in the volume of the glass network due to the incorporation of 4- and 5-coordinated V^{5+} and V^{4+} units in its structure [53], as discussed in Section 4.

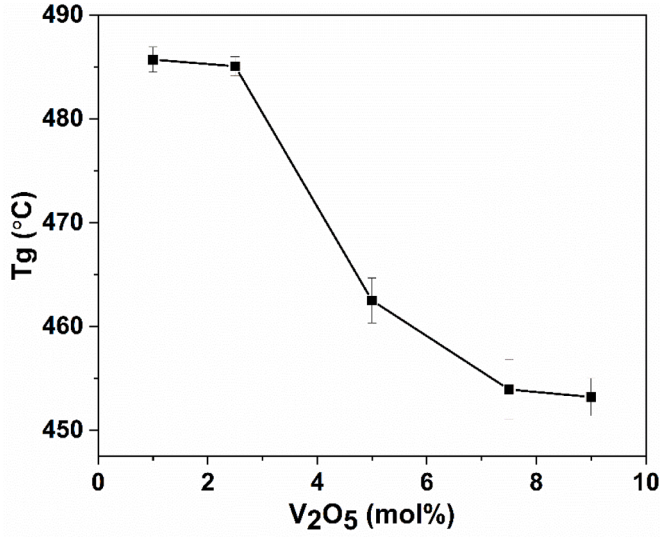

Fig. 6. Variation of glass transition temperature (T_g) of *x*V glass as a function of V_2O_5 concentration.

3.3. Sulfur solubility in glasses and its impact on glass structure and properties

3.3.1. Sulfur solubility in glasses

Sulfur (as SO_3) has been added to the *x*V glasses (starting from 1 mol. % SO_3) until it supersaturates in the melt and appears as a salt layer on the glass surface. The highest concentration of SO_3, which dissolves in a glass without altering its amorphous nature (as analyzed by XRD analysis), has been defined as its solubility limit. Once the SO_3 solubility limit has been reached, the excess sulfate tends to partition out of the melt in the form of salt and floats on the melt surface. Upon quenching the melt, the salt layer tends to stick to the surface of the transparent and XRD amorphous glass. All the sulfur-containing glasses (within the solubility limit) are XRD amorphous, as shown in Fig. 8a. Interestingly, the color of the salt layer, formed after the supersaturation of SO_3 in the glass melt, changes from white to brown as V_2O_5 content increases in the investigated glasses. The XRD analysis of the white salt reveals the formation of Na_2SO_4 [PDF# 04–009–1822; Orthorhombic, Space group: Cmcm (63)] as the only phase, while the brown salt exhibits the presence of a small fraction of Na_2SO_4 [PDF# 98–000–0433; Orthorhombic; Space group: Fddd (70)] and $NaVO_3$ (PDF# 04–013–7267) along with Na_2SO_4 (PDF# 04–009–1822), as evident from Fig. 8b.

Table 1 presents the compositions of the sulfur-free (*x*V) and sulfur-containing (*x*V-*y*S) glasses, as analyzed by ICP-OES. The compositional analysis of the sulfur-containing glasses has been performed only for the compositions supersaturated with SO_3. Therefore, the SO_3 concentrations reported in Table 1 should be considered as the solubility limit of sulfate ions in the respective glasses under the given experimental conditions. The experimental compositions of the sulfur-free glasses are in good agreement with the batched compositions, suggesting minimal volatility of Na_2O or B_2O_3 from the glass melts.

The addition of ≤5 mol.% V_2O_5 to the baseline glass results in a linear increase in the SO_3 solubility (Fig. 9), from 1 mol.% in 0 V glass to 3 mol.% in 5 V glass. Here, it should be noted that the SO_3 addition to these glasses did not significantly change their physical appearance, as evident from Fig. 1. An increase in V_2O_5 concentration to 7.5 mol.% in the baseline glass doubled the SO_3 solubility (compared to 5 V glass) to

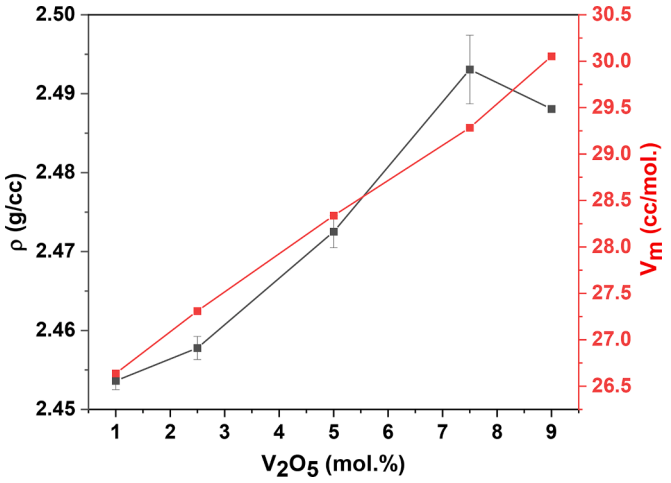

Fig. 7. Variation of density (ρ) and molar volume (V_m) of *x*V glass as a function of V_2O_5 concentration.

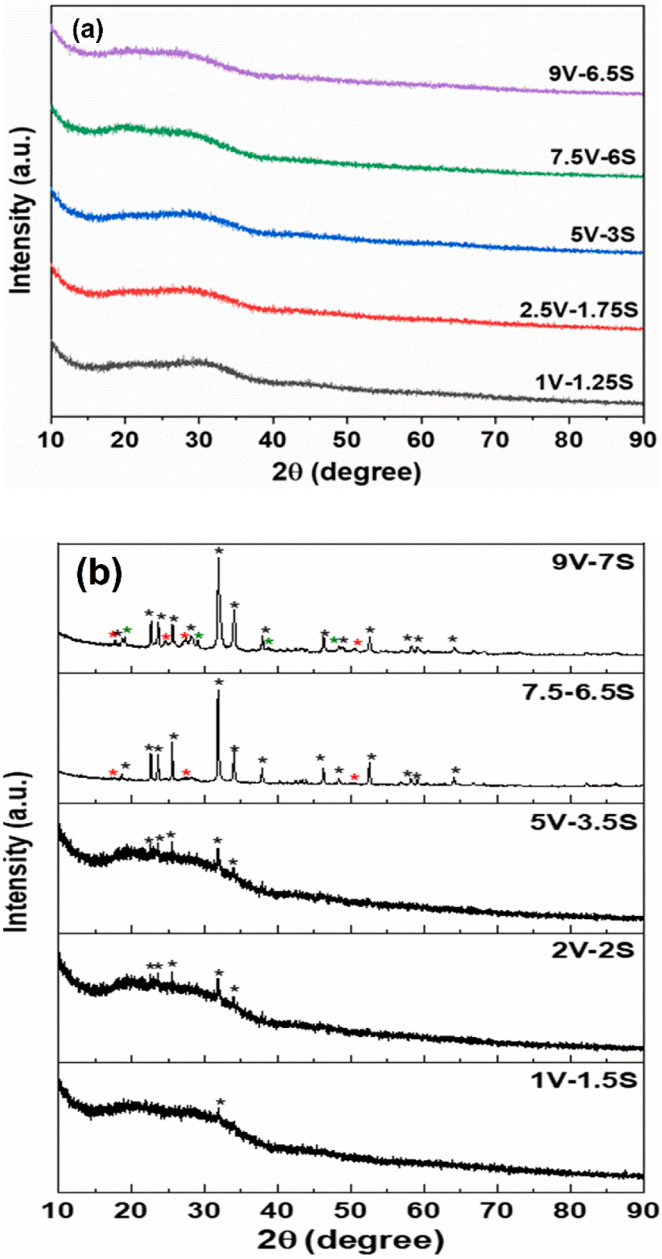

Fig. 8. (a) Sulfur-containing glasses (within solubility limit) and (b) Na_2SO_4 (in case of 1 V, 2.5 V, 5 V glass) while Na_2SO_4 (*), minor Thenardite (*) and $NaVO_3$ (*) crystalline phases observed as salt layer over the surface of phase separated 7.5 V and 9 V glasses.

6 mol.%. However, the addition of 6.5 mol.% SO_3 to 7.5 V glass induced visible phase separation in the glass, as shown in Fig. 1. Further increase in V_2O_5 concentration to 9 mol.% did not significantly impact the SO_3 solubility, as evidenced by Table 1.

3.3.2. *Impact of sulfur on the structure and properties of glasses*

Sulfur is known to exist in glasses with valence states ranging from S^{2-} (sulfide) to S^{6+} (sulfate), depending on the redox chemistry of the glass melt [19,61,62]. Polysulfide chains or rings would give rise to S–S stretching modes in the region 300–460 cm^{-1}, while two closely spaced bands in the 950–970 and 970–990 cm^{-1} regions would be expected for SO_3^{2-} (sulfite) groups [63–65]. For the glasses investigated in the present study, we found no evidence of sulfur speciation with an oxidation state other than +6, i.e., sulfur exclusively exists as a sulfate (SO_4^{2-}) species in

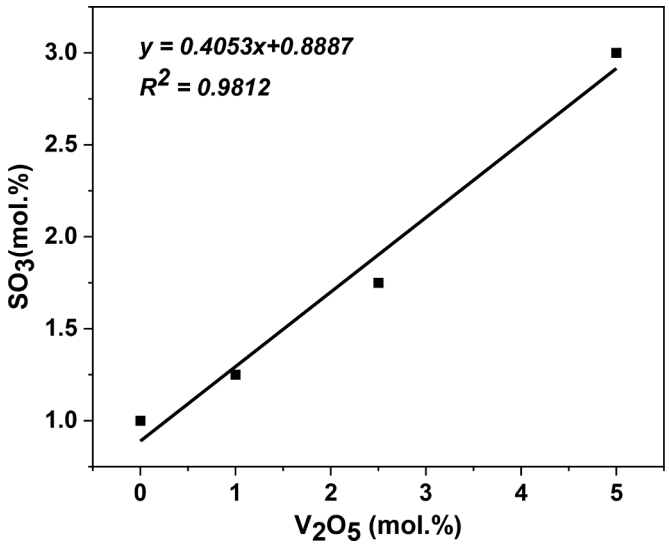

Fig. 9. A linear increase in SO_3 solubility in glasses with increasing V_2O_5 content up to 5 mol.%.

the investigated glasses. A comparison of the Raman spectra of sulfur-free and sulfur-containing 1 V glass has been presented in Fig. 10a as a representative example to depict the speciation of sulfur in the investigated glasses.

Two new bands can be seen to evolve in the Raman spectra of sulfur-containing glasses: the increased intensity band component near 460 cm^{-1}, corresponding to asymmetric O–S–O bending modes, and a band at 988 cm^{-1} attributed to symmetric S–O stretching modes. While the group theoretical analysis predicts four vibrational modes assigned as: ν_1 (symmetric S–O stretching modes) at ~990 cm^{-1}; ν_2 (symmetric O–S–O bending modes) at ~460 cm^{-1}; ν_3 (asymmetric S–O stretching modes) at ~1100 cm^{-1}; and ν_4 (asymmetric O–S–O bending modes) at ~620 cm^{-1} [2,12], only the bands corresponding to the modes characterized by the frequencies ν_1 and ν_2 are visible. The other two modes are difficult to identify because they overlap with bands attributed to vibrational modes associated with the borosilicate network. In the present work, the sharp band at 987 cm^{-1} in the glass samples has been taken as the fingerprint of the presence of sulfur as SO_4^{2-} in the investigated glasses, and its intensity increases with an increase in SO_3 concentration [20].

The introduction of SO_4^{2-} anions in the glass network leads to the re-polymerization of the glass network, as indicated by the slight shift of the Q^3 peak towards a higher frequency, along with the increase in the intensity of the Q^4 edge in the range 1100–1200 cm^{-1}. Basically, the incorporated SO_4^{2-} anions can scavenge Na^+ from non-bridging oxygen (NBO) containing borate and silicate units, thereby re-polymerizing these parts of the glass network [2]. The SO_4^{2-} cannot scavenge Na^+ from BO_4^- or AlO_4^- units [10,20]. In the present study, based on Raman spectroscopy data, the possibility of SO_4^{2-} to scavenge Na^+ from anionic BO_3 (i.e., BO_3 with non-bridging oxygen) units is negligible. Therefore, as a first approximation, the re-polymerization of the glass network is primarily due to the formation of Si–O–Si linkages in the glass network, decreasing the concentration of NBO and increasing the T_g of sulfur-containing glass as compared to the sulfur-free glass (Fig. 10b). Here it needs to be mentioned that we have not considered the possibility of SO_4^{2-} scavenging Na^+ from vanadate ions as, according to the literature, sulfate, and V^{5+} do not interact with each other in the structure of borosilicate glasses [24,66].

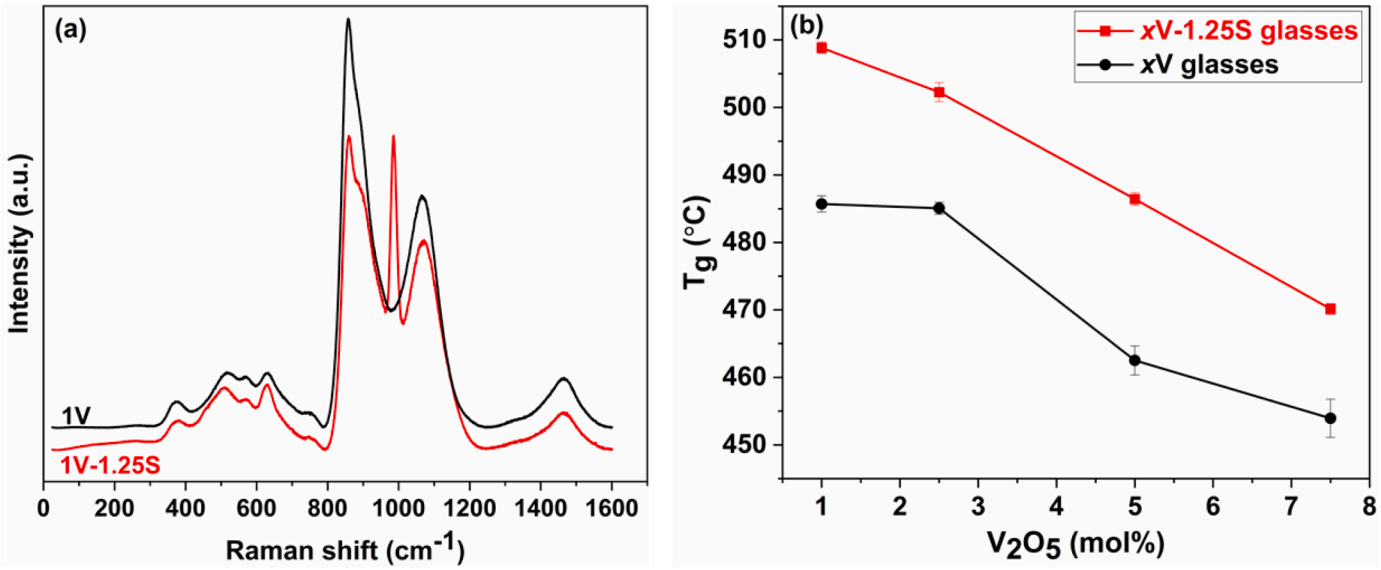

Fig. 10. (a) Comparison of Raman spectra of 1 V and 1V-1.25S glasses, and (b) comparison of T_g of *x*V and *x*V-1.25S glasses.

4. Discussion

4.1. Compositional dependence of redox chemistry of vanadium

Vanadium can co-exist in an alkali aluminoborosilicate glass in the following three different oxidation states: V^{3+}, $V^{4+,}$ and V^{5+}, where V^{4+} and V^{5+} tend to act as the first redox pair and V^{3+} and V^{4+} act as the second redox pair, as described in Eqs. (2) and (3), respectively [67,68].

$$2O^{2-} + 4V^{5+} \rightleftharpoons 4V^{4+} + O_2 \quad (2)$$

$$2O^{2-} + 4V^{4+} \rightleftharpoons 4V^{3+} + O_2 \quad (3)$$

In peralkaline glasses (Na/Al > 1) synthesized in an ambient atmosphere, V^{5+} is the dominant species (>90%) followed by V^{4+} (<10%). The V^{3+} species has been shown to be present in trace quantities (<1%) in peralkaline glasses. However, the concentration of both V^{3+} and V^{4+} increases when the glass composition shifts from peralkaline to peraluminous [35,68,69]. In other words, the basicity of a glass has a significant impact on the redox chemistry of vanadium in the glass melt, i.e., alkaline glasses favor the more acidic (+5) state of vanadium. As the acidity of the glass is increased, the more basic (lower) state of vanadium is favored [32]. Therefore, considering the peralkaline nature of the glasses in the present study, the dominance of +5 oxidation state of vanadium is not surprising.

Further, an increase in the V^{4+}/V^{5+} ratio in glasses with $V_2O_5 \geq 5$ mol.% may be explained based on the thermodynamic redox equilibrium of a polyvalent ion (M^{x+}) in an oxide glass melt under an ambient atmosphere, as described by the general Eq. (4),

$$2O^{2-} + \frac{4}{n}M^{(x+n)+} \rightleftarrows \frac{4}{n}M^{(x)+} + O_2 \quad (4)$$

where *n* represents the change in the number of electrons in the oxidation–reduction reaction, and O_2 is the oxygen dissolved in the glass melt. Since the redox reactions of polyvalent ions in a glass melt are endothermic and can be adjusted by varying its melting temperature and partial pressure of oxygen (pO_2), high melting temperatures or low pO_2 can shift the redox ratios to more reduced states [70]. In the present study, the addition of V_2O_5 is expected to lower the melting temperatures (T_m) of the glasses – based on the empirical relation proposed by Kauzmann (Eq. (5)) [71].

$$T_m = \frac{3}{2}T_g \quad (5)$$

However, all the glass melts in the present study are heated at 1200 °C for 1 h. Thus, the glasses with higher V_2O_5 content, for example, 7.5 V or 9 V, have encountered relatively higher melting temperatures compared to the glasses with lower V_2O_5 content, thus shifting the reaction in Eq. (2) toward the right-hand side.

4.2. Impact of vanadium redox on the glass structure

The impact of the redox chemistry of vanadium on the structure of borosilicate glasses is still debatable. According to Lu et al. [53], V^{5+} can exist in 4, 5, and 6-coordination in the structure of a peralkaline glass, while V^{4+} mainly exists in 4-fold coordination, with minor fractions of 5- and 6-coordinated species. However, their results are based on molecular dynamic simulations and have not been experimentally validated. The experimental studies (literature) suggest that vanadium exists in peralkaline borosilicate glasses primarily as $V^{5+}O_4$ units (vanadate), with a small fraction of $V^{4+}O_5$ units (cavansite) [2,28,35,66,72]. Therefore, though we are not negating the possibility of 4+ and 5+ vanadium species in multiple coordination states in the glass structure, we have based our discussion on the results demonstrated experimentally in the literature.

When discussing the impact of V_2O_5 on the structure of the investigated glasses, ^{27}Al MAS NMR spectra of the sulfur-free *x*V glasses (Fig. 5a) reveal that the atomic abundance of A^{IV} units does not change with V_2O_5 addition (Table 2), which is consistent with the reported literature [48,72]. This can be explained based on the following two hypotheses: (1) AlO_4^- prefers to be charge compensated by Na^+ over $[V^{5+}O_4]^{+1}$. Since there is sufficient Na^+ available to charge-compensate AlO_4^-, the addition of V_2O_5 does not affect the aluminum coordination in the glass structure; (2) $[V^{5+}O_4]^{+1}$ replaces or competes effectively with Na^+ for the charge compensation of AlO_4^-, thus, resulting in the formation of Al–O–V linkages or $AlVO_4$ neutral units analogous to Al–O–P or $AlPO_4$ units in P_2O_5 containing glasses [50]. Owing to a minimal shift in the ^{27}Al MAS NMR spectra of the investigated glasses with increasing V_2O_5 concentration (not surprising due to the highly peralkaline nature of glasses), we expect the first hypothesis, i.e., Na^+ charge compensating AlO_4^-, to be the most likely reason for a constant AlO_4 concentration. The charge compensation of AlO_4^- units by $[V^{5+}O_4]^{+1}$ can be hypothesized in the peraluminous glasses, as has also been proposed by Cicconi et al.

[35], which are quite distinct from the compositions explored in this work.

On the other hand, an increase in the fraction of B^{IV} units with increasing V_2O_5 concentration (up to 7.5 mol.%) followed by a decrease with a further increase in V_2O_5 concentration to 9 mol.% suggests an interaction between the V^{4+}, V^{5+}, and borate units in the glass structure. Similar trends for borate speciation as a function of V_2O_5 content have been reported for lithium borovanadate [48,73], binary vanadium borate [60], borosilicate [27], and aluminoborosilicate [53,72] glasses. However, the exact nature of these interactions leading to these trends is still unclear and needs further investigation. According to Lu et al. [53], $[V^{5+}O_4]^{+1}$ acts as a modifier in the glass network. In glasses with lower V_2O_5 content, it acts as a charge compensator to facilitate the conversion of BO_3 to BO_4 units. At higher V_2O_5 concentrations, it starts to create NBOs instead of facilitating $B^{III} \rightarrow B^{IV}$ conversion. The above-mentioned explanation by Lu et al. [53] contradicts their own results in the same article, where they also classify $[V^{5+}O_4]$ units as a network former in the glass structure. Another plausible explanation for the initial increase and then a decrease in the fraction of BO_4 units with an increasing concentration of V_2O_5 has been proposed by Muthupari et al. [54] in sodium borovanadate glasses. According to Muthupari et al. [54], the formation of BO_4 units in the borovanadate glasses occurs in pairs via the bridging of BO_3 units by an O^{2-} ion resulting in the formation of diborovanadate type species with the formula $[B_2V_2O_9]^{2-}$. They did not observe the formation of $[BO_{3/2}O]^-$ type B^{IV} units. Whether similar vanadium-containing borate or borosilicate-based superstructural units are formed in borosilicate glasses needs to be seen. Therefore, as mentioned above, additional spectroscopic investigations need to be performed to unearth the exact reason for the observed trends pertaining to borate speciation in the investigated glasses as a function of V_2O_5 content.

The impact of V_2O_5 addition to the silicate network of the glass structure is based on the analysis of Raman spectra (Fig. 4), wherein the 800 cm^{-1} – 1200 cm^{-1} region corresponding to the stretching vibrations of Q^n units is heavily masked by the bands corresponding to the vibration of VO_x units. Therefore, it is difficult to draw any quantitative trends pertaining to the change in the degree of polymerization in the silicate network of glasses as a function of V_2O_5 content. Nonetheless, based on the molar volume results and the trends observed in the Raman spectra of glasses as a function of V_2O_5 content, we hypothesize the formation of Si–O–V type weaker linkages in the glass structure at the expense of Si–O–Si stronger linkages. Here, it should be mentioned that the authors could not find any literature demonstrating the interaction of V^{5+} with the silicate network in the glasses; though V^{4+}–O–Si linkages have been reported in mineral canavsite [$Ca(VO)Si_4O_{10}\bullet 4H_2O$] [24,74]. Nevertheless, the possibility of existence of Si–O–V^{5+} linkages in the glass structure cannot be negated as $V^{5+}O_4$ and SiO_4 units co-exist as a solid solution in the naturally existing mineral aradite [$BaCa_6[(SiO_4)(VO_4)](VO_4)_2F$] [75]. Therefore, further detailed structural studies on this subject are warranted.

4.3. Impact of glass structure on SO_4^{2-} solubility

The sulfate (SO_4^{2-}) solubility in a borosilicate glass depends on two factors: (1) the presence of voids or depolymerized regions in the glass structure to accommodate the SO_4^{2-} tetrahedra and (2) the availability of network modifier cations to charge compensate the accommodated SO_4^{2-} tetrahedra [2,11,14,20,21,24,61]. In the present study, the addition of V_2O_5 results in an increase in the molar volume of the glasses, which according to Lu et al. [64], is the reason for higher sulfur solubility in vanadium-containing borosilicate glasses. This, in our opinion, is incorrect because higher molar volume indicates more directional bonding in the glass network [44,76], thus resulting in lower sulfur solubility, as has been shown in our previous study [20]. Another factor that can be attributed to the higher sulfur solubility in vanadium-containing borosilicate glasses is network depolymerization. According to Sengupta et al. [27], with the addition of $\leq$5 mol.% V_2O_5, the borate network in the glass structure tends to depolymerize, while the silicate network remains unaltered, thus increasing the sulfur solubility. This is contrary to their own ^{11}B MAS NMR results where it has been shown that the addition of $\leq$5 mol.% V_2O_5 results in an increase in the fraction of BO_4 units in the glassy matrix [27]. Further, according to Manara et al. [2], the higher sulfur solubility in vanadium-containing sodium borosilicate glasses is due to the depolymerization of silicate and borate networks induced by a high alkali content and/or the presence of vanadium-oxygen chains, that lead to the creation of voids in the borosilicate matrix. The mechanism proposed by Manara et al. [2], is justified as they vary the alkali–to–network former ratio in their glass compositions with a fixed V_2O_5 content. However, their results cannot be compared with the present study as we are increasing V_2O_5 content in glasses with the molar ratios of all other oxides in the glass composition being constant.

In our opinion, an increased sulfur solubility in borosilicate glasses is due to a net decrease in the network rigidity of the glass structure as described here: A fraction of $V^{5+}O_4$ units in the glass structure organize themselves as $(VO_3)_n$-single chains, as proposed by Manara et al. [2] (in borosilicate glasses) and Hayakawa et al. [77] (in alkaline-earth vanadate glasses), thus increasing the network connectivity in the glass structure, resulting in higher molar volume. This assertion is supported by the formation of $NaVO_3$ phase in the salt layer of V_2O_5-rich glass melts supersaturated with SO_4^{2-}. On the other hand, the remaining $V^{5+}O_4$ units weaken the silicate network by replacing Si–O–Si linkages with Si–O–V linkages. These modifications to the glass structure decrease the overall network rigidity [78,79], thus making it possible to accommodate SO_4^{2-} in their voids/open spaces. Here it needs to be mentioned that the (1) possibility of the existence of $(VO_3)_n$-single chains is a hypothesis that contradicts the concept of isolated $(VO_4)^{3-}$ proposed by McKeown et al. [80], thus, warrants further experimental structural investigations; (2) reason for a 2 × increase in SO_3 solubility in glasses upon increasing V_2O_5 content from 5 mol.% to 7.5 mol.% is still unclear and needs to be investigated further.

The next question is how the incorporated SO_4^{2-} anionic units are charge-compensated in the glass network. According to Lu et al. [53], $[V^{5+}O_4]^{+1}$ acts as a charge compensator for SO_4^{2-} tetrahedral units. However, as has been experimentally shown by McKeown et al. [24,66], vanadium and sulfur do not interact in the structure of borosilicate glasses. Also, the segregation of SO_4^{2-} and VO_3^- (where V is in +5 oxidation state) oxyanions in the melts supersaturated with sulfur, where both the oxyanions are being charge compensated by Na^+ (resulting in the formation of Na_2SO_4 and $NaVO_3$ salt phases), demonstrate that vanadium and sulfur do not interact with each other in the glass structure, thus refuting the proposition of Lu et al. [53]. The hypothesis of charge compensation of SO_4^{2-} by Na^+ is also supported by an increase in the T_g of the sulfur-containing glasses (Fig. 10b), thus suggesting re-polymerization in the glass structure, as has been shown in our previous studies [10,20].

5. Conclusion

A suite of state-of-the art spectroscopic techniques have been employed to decipher the origin of increased sulfur solubility in borosilicate glasses as a function of V_2O_5 content. Vanadium primarily exists as V^{5+} (as $V^{5+}O_4$) in the investigated glasses with a small fraction of V^{4+} (whose fraction increases with increasing V_2O_5 concentration). The addition of V_2O_5 (up to 9 mol.%) to the baseline glass (0 V) results in (1) a minimal change in the aluminum coordination suggesting the charge compensation of AlO_4 units by Na^+; (2) an increase in the fraction of BO_4 units until 7.5 mol.% V_2O_5 followed by a decrease with further increase in V_2O_5 concentration to 9 mol.% — further investigations are needed to understand the origin of this trend; (3) an increased connectivity but decreased rigidity of the glass network. In our opinion, it is the decreased rigidity of the glass network that makes it possible to

accommodate SO_4^{2-} in their voids/open spaces, thus resulting in an increased sulfur solubility.

Declaration of Competing Interest

The authors declare that they have no known competing financial interests or personal relationships that could have appeared to influence the work reported in this paper.

Data availability

Data will be made available on request.

Acknowledgement

This material is based upon work supported by funding provided by the US Department of Energy (DOE), Office of River Protection, Waste Treatment & Immobilization Plant (WTP), through contract numbers 89304018CEM000006 and 89304022CEM000015, and the National Science Foundation under Grant No. 2034871.

References

[1] A.A. Kruger, Advances in Glass Formulations For Hanford high-aluminum, High-Iron and Enhanced Sulfate Management in HLW Streams - 13000, in, United States, 2013.
[2] D. Manara, A. Grandjean, O. Pinet, J.L. Dussossoy, D.R. Neuville, Sulfur behavior in silicate glasses and melts: Implications for sulfate incorporation in nuclear waste glasses as a function of alkali cation and V_2O_5 content, J. Non-Cryst. Solids 353 (2007) 12–23.
[3] C.H. Skidmore, J.D. Vienna, T. Jin, D. Kim, B.A. Stanfill, K.M. Fox, A.A. Kruger, Sulfur solubility in low activity waste glass and its correlation to melter tolerance, Int. J. Appl. Glass Sci. 10 (2019) 558–568.
[4] J.D. Vienna, D.S. Kim, I.S. Muller, G.F. Piepel, A.A. Kruger, Toward understanding the effect of low-activity waste glass composition on sulfur solubility, J. Am. Ceram. Soc. 97 (2014) 3135–3142.
[5] C.P. Kaushik, R.K. Mishra, V. Thorat, M. Ramchandran, K. Amar, P.D. Ozarde, K. Raj, D. Das, Development of a Glass Matrix For Vitrification of Sulphate Bearing High Level Radioactive Liquid waste, (BARC-2004/E/018), Bhabha Atomic Research Center, India, 2004, p. 19.
[6] C.P. Kaushik, Indian program for vitrification of high level radioactive liquid waste, Proc. Mater. Sci. 7 (2014) 16–22.
[7] L.J. Liu, J.H. Xu, Y.Z. Jiang, Study on sulfate phase segregation and decomposition in vitrification process, Atom. Energ. Sci. Tech. 49 (2015) 1551.
[8] T. Jin, D. Kim, L.P. Darnell, B.L. Weese, N.L. Canfield, M. Bliss, M.J. Schweiger, J. D. Vienna, A.A. Kruger, A crucible salt saturation method for determining sulfur solubility in glass melt, Int. J. Appl. Glass Sci. 10 (2019) 92–102.
[9] P.A. Bingham, S. Vaishnav, S.D. Forder, A. Scrimshire, B. Jaganathan, J. Rohini, J. C. Marra, K.M. Fox, E.M. Pierce, P. Workman, J.D. Vienna, Modelling the sulfate capacity of simulated radioactive waste borosilicate glasses, J. Alloys Comp. 695 (2017) 656–667.
[10] R. Saini, S. Kapoor, D.R. Neuville, R.E. Youngman, B.M. Cerrutti, J.S. McCloy, H. Eckert, A. Goel, Correlating sulfur solubility with short-to-intermediate range ordering in the structure of borosilicate glasses, J. Phys. Chem. C 126 (2022) 655–674.
[11] D.A. McKeown, I.S. Muller, H. Gan, I.L. Pegg, W.C. Stolte, Determination of sulfur environments in borosilicate waste glasses using X-ray absorption near-edge spectroscopy, J. Non-Cryst. Solids 333 (2004) 74–84.
[12] D.A. McKeown, I.S. Muller, H. Gan, I.L. Pegg, C.A. Kendziora, Raman studies of sulfur in borosilicate waste glasses: sulfate environments, J. Non-Cryst. Solids 288 (2001) 191–199.
[13] D.A. McKeown, I.S. Muller, A.C. Buechele, I.L. Pegg, C.A. Kendziora, Structural characterization of-high-zirconia borosilicate glasses using Raman spectroscopy, J. Non-Cryst. Solids 262 (2000) 126–134.
[14] J.M. Lonergan, C. Lonergan, J. Silverstein, P. Cholsaipant, J. McCloy, Thermal properties of sodium borosilicate glasses as a function of sulfur content, J. Am. Ceram. Soc. 103 (2020) 3610–3619.
[15] I.S. Muller, K. Gilbo, M. Chaudhuri, I.L. Pegg, I. Joseph, K-3 Refractory corrosion and sulfate solubility model enhancement (Final Report), in, United States, 2018. DOI: 10.2172/1513833.
[16] A.A. Kruger, I.L. Pegg, K.S. Matlack, I. Joseph, I.S. Muller, W. Gong, Final Report - Enhanced LAW Glass Formulation Testing, VSL-07R1130-1, Rev. 0, dated 10/05/07, in, United States, 2013. DOI: 10.2172/1105974.
[17] X. Xu, T. Han, J. Huang, A.A. Kruger, A. Kumar, A. Goel, Machine learning enabled models to predict sulfur solubility in nuclear waste glasses, ACS Appl. Mater. Interfaces 13 (2021) 53375–53387.
[18] S.V. Stefanovskii, Glasses for immobilization of sulfur containing radioactive waste, Radiokhimiya 31 (1989) 129–134.
[19] M. Lenoir, A. Grandjean, S. Poissonnet, D.R. Neuville, Quantitation of sulfate solubility in borosilicate glasses using Raman spectroscopy, J. Non-Cryst. Solids 355 (2009) 1468–1473.
[20] X. Xu, R.E. Youngman, S. Kapoor, A. Goel, Structural drivers controlling sulfur solubility in alkali aluminoborosilicate glasses, J. Am. Ceram. Soc. 104 (2021) 5030–5049.
[21] S. Vaishnav, A.C. Hannon, E.R. Barney, P.A. Bingham, Neutron diffraction and Raman studies of the incorporation of sulfate in silicate glasses, J. Phys. Chem. C 124 (2020) 5409–5424.
[22] A. Krishnamurthy, S. Kroeker, Improving molybdenum and sulfur vitrification in borosilicate nuclear waste glasses using phosphorus: Structural insights from NMR, Inorg. Chem. 61 (2022) 73–85.
[23] R.K. Mishra, K.V. Sudarsan, P. Sengupta, R.K. Vatsa, A.K. Tyagi, C.P. Kaushik, D. Das, K. Raj, Role of sulfate in structural modifications of sodium barium borosilicate glasses developed for nuclear waste immobilization, J. Am. Ceram. Soc. 91 (2008) 3903–3907.
[24] D.A. McKeown, I.S. Muller, K.S. Matlack, I.L. Pegg, X-ray absorption studies of vanadium valence and local environment in borosilicate waste glasses using vanadium sulfide, silicate, and oxide standards, J. Non-Cryst. Solids 298 (2002) 160–175.
[25] N. Smith-Gray, J. Lonergan, J. McCloy, Chromium and vanadium incorporation in sulfate-containing sodium aluminoborosilicate glass, MRS Adv 6 (2021) 138–148.
[26] N. Stone-Weiss, H. Bradtmüller, M. Fortino, M. Bertani, R.E. Youngman, A. Pedone, H. Eckert, A. Goel, Combined experimental and computational approach toward the structural design of borosilicate-based bioactive glasses, J. Phys. Chem. C 124 (2020) 17655–17674.
[27] P. Sengupta, K.K. Dey, R. Halder, T.G. Ajithkumar, G. Abraham, R.K. Mishra, C. P. Kaushik, G.K. Dey, Vanadium in borosilicate glass, J. Am. Ceram. Soc. 98 (2015) 88–96.
[28] X. Lu, R. Sun, L. Huang, J.V. Ryan, J.D. Vienna, J. Du, Effect of vanadium oxide addition on thermomechanical behaviors of borosilicate glasses: Toward development of high crack resistant glasses for nuclear waste disposal, J. Non-Cryst. Solids 515 (2019) 88–97.
[29] R.K. Harris, E.D. Becker, S.M. Cabral de Menezes, P. Granger, R.E. Hoffman, K.W. Zilm, Further conventions for NMR shielding and chemical shifts (IUPAC Recommendations 2008), 80 (2008) 59–84.
[30] J.H. Scofield, Theoretical Photoionization Cross Sections from 1 to 1500 KeV, California Univ., Livermore. Lawrence Livermore Lab., 1973.
[31] G.C. Smith, Evaluation of a simple correction for the hydrocarbon contamination layer in quantitative surface analysis by XPS, J. Electron Spectros. Relat. Pheno. 148 (2005) 21–28.
[32] W.A. Weyl, A.G. Pincus, A.E. Badger, Vanadium as a glass colorant, J. Am. Ceram. Soc. 22 (1939) 374–377.
[33] B. Mirhadi, B. Mehdikhani, Investigation of optical absorbance and crystallization of vanadium oxide in glasses, J. Optoelectron. Adv. Mater. 13 (2011) 679.
[34] R. Halder, P. Sengupta, V. Sudarsan, C.P. Kaushik, G.K. Dey, Investigating the effect of V_2O_5 addition on sodium barium borosilicate glasses, AIP Conf. Proc. 1731 (2016), 070005.
[35] M.R. Cicconi, Z. Lu, T. Uesbeck, L. van Wüllen, D.S. Brauer, D. de Ligny, Influence of vanadium on optical and mechanical properties of aluminosilicate glasses, Front. Mater. 7 (2020) 161.
[36] M.C. Biesinger, L.W.M. Lau, A.R. Gerson, R.S.C. Smart, Resolving surface chemical states in XPS analysis of first row transition metals, oxides and hydroxides: Sc, Ti, V, Cu and Zn, Appl. Surf. Sci. 257 (2010) 887–898.
[37] D. Manara, A. Grandjean, D. Neuville, Advances in understanding the structure of borosilicate glasses: A Raman spectroscopy study, Am. Mineral. 94 (2009) 777–784.
[38] C.Le Losq, D.R. Neuville, P. Florian, G.S. Henderson, D. Massiot, The role of Al^{3+} on rheology and structural changes in sodium silicate and aluminosilicate glasses and melts, Geochim. Cosmochim. Acta 126 (2014) 495–517.
[39] B. Cochain, D.R. Neuville, G.S. Henderson, C.A. McCammon, O. Pinet, P. Richet, Effects of the iron content and redox state on the structure of sodium borosilicate glasses: A Raman, Mössbauer and boron K-Edge XANES spectroscopy study, J. Am. Ceram. Soc. 95 (2012) 962–971.
[40] L. Cormier, D. Meneses, D. Neuville, P. Echegut, In situ evolution of the structure of alkali borate glasses and melts by infrared reflectance and Raman spectroscopies, Phys. Chem. Glasses 47 (2006) 430–434.
[41] M. Lenoir, A. Grandjean, Y. Linard, B. Cochain, D.R. Neuville, The influence of Si, B substitution and of the nature of network-modifying cations on the properties and structure of borosilicate glasses and melts, Chem. Geol. 256 (2008) 316–325.
[42] D. de Waal, C. Hutter, Vibrational spectra of two phases of copper pyrovanadate and some solid solutions of copper and magnesium pyrovanadate, Mater. Res. Bull. 29 (1994) 843–849.
[43] A. Paul, Physical Properties, in: A. Paul (Ed.), Chemistry of Glasses, Springer Netherlands, Dordrecht, 1982, pp. 51–107.
[44] J.W. Martin, Concise Encyclopedia of the Structural Materials, Elsevier Science, 2006.
[45] A. Brehault, D. Patil, H. Kamat, R.E. Youngman, L.M. Thirion, J.C. Mauro, C. L. Corkhill, J.S. McCloy, A. Goel, Compositional dependence of solubility/retention of molybdenum oxides in aluminoborosilicate-based model nuclear waste glasses, J. Phys. Chem. B 122 (2018) 1714–1729.
[46] S. Kapoor, R.E. Youngman, K. Zakharchuk, A. Yaremchenko, N.J. Smith, A. Goel, Structural and chemical approach toward understanding the aqueous corrosion of sodium aluminoborate glasses, J. Phys. Chem. B 122 (2018) 10913–10927.

[47] N. Stone-Weiss, R.E. Youngman, R. Thorpe, N.J. Smith, E.M. Pierce, A. Goel, An insight into the corrosion of alkali aluminoborosilicate glasses in acidic environments, Phys. Chem. Chem. Phys. 22 (2020) 1881–1896.
[48] M. Kindle, S. Kmiec, I. d'Anciães Almeida Silva, H. Eckert, S.W. Martin, M.K. Song, J.S. McCloy, Structural properties of alumina-doped lithium borovanadate glasses and glass-ceramics, J. Non-Cryst. Solids 521 (2019), 119551.
[49] P. Lu, S. Kapoor, L. Kobera, J. Brus, A. Goel, Structural dependence of crystallization in phosphorus-containing sodium aluminoborosilicate glasses, J. Am. Ceram. Soc. 105 (2022) 2556–2574.
[50] P. Lu, Y. Zan, J. Ren, T. Zhao, K. Xu, A. Goel, Structure and crystallization behavior of phosphorus-containing nepheline ($NaAlSiO_4$) based sodium aluminosilicate glasses, J. Non-Cryst. Solids 560 (2021), 120719.
[51] L.S. Du, J.F. Stebbins, Solid-state NMR study of metastable immiscibility in alkali borosilicate glasses, J. Non-Cryst. Solids 315 (2003) 239–255.
[52] L.S. Du, J.F. Stebbins, Site preference and Si/B mixing in mixed-alkali borosilicate glasses: a high-resolution ^{11}B and ^{17}O NMR study, Chem. Mater. 15 (2003) 3913–3921.
[53] X. Lu, L. Deng, S.A. Saslow, H. Liu, C.J. Benmore, B.P. Parruzot, J.T. Reiser, S. H. Kim, J.V. Ryan, J.D. Vienna, J. Du, Vanadium oxidation states and structural role in aluminoborosilicate glasses: An integrated experimental and molecular dynamics simulation study, J. Phys. Chem. B 125 (2021) 12365–12377.
[54] S. Muthupari, S. Prabakar, K.J. Rao, Chemical Basis of the structural modification in sodium borovanadate glasses. Thermal and spectroscopic studies, J. Phys. Chem. 98 (1994) 2646–2652.
[55] N.S. Saetova, A.A. Raskovalov, B.D. Antonov, T.A. Denisova, N.A. Zhuravlev, Structural features of Li_2O–V_2O_5–B_2O_3 glasses: Experiment and molecular dynamics simulation, J. Non-Cryst. Solids 545 (2020), 120253.
[56] G. Tricot, L. Montagne, L. Delevoye, G. Palavit, V. Kostoj, Redox and structure of sodium-vanadophosphate glasses, J. Non-Cryst. Solids 345 (2004) 56–60.
[57] A. Gaddam, A.R. Allu, H.R. Fernandes, G.E. Stan, C.C. Negrila, A.P. Jamale, F. O. Méar, L. Montagne, J.M.F. Ferreira, Role of vanadium oxide on the lithium silicate glass structure and properties, J. Am. Ceram. Soc. 104 (2021) 2495–2505.
[58] J. Skibsted, N.C. Nielsen, H. Bildsoe, H.J. Jakobsen, Magnitudes and relative orientation of vanadium-51 quadrupole coupling and anisotropic shielding tensors in metavanadates and potassium vanadium oxide (KV_3O_8) from vanadium-51 MAS NMR spectra. Sodium-23 quadrupole coupling parameters for α- and β-$NaVO_3$, J. Am. Chem. Soc. 115 (1993) 7351–7362.
[59] G. Adam, J.H. Gibbs, On the temperature dependence of cooperative relaxation properties in glass-forming liquids, J. Chem. Phys. 43 (1965) 139–146.
[60] N. Laorodphan, P. Pooddee, P. Kidkhunthod, P. Kunthadee, W. Tapala, R. Puntharod, Boron and pentavalent vanadium local environments in binary vanadium borate glasses, J. Non-Cryst. Solids 453 (2016) 118–124.
[61] M. Lenoir, D.R. Neuville, M. Malki, A. Grandjean, Volatilization kinetics of sulphur from borosilicate melts: A correlation between sulphur diffusion and melt viscosity, J. Non-Cryst. Solids 356 (2010) 2722–2727.
[62] M. Lenoir, Sulphate Solubility and Sulphate Diffusion in Oxide glasses: Implications For the Containment of Sulphate-Bearing Nuclear Wastes, in, France, 2009, pp. 257.
[63] A.T. Ward, Raman spectroscopy of sulfur, sulfur-selenium, and sulfur-arsenic mixtures, J. Phys. Chem. 72 (1968) 4133–4139.
[64] C. Sourisseau, R. Cavagnat, M. Fouassier, The vibrational properties and valence force fields of FeS_2, RuS_2 pyrites and FeS_2 marcasite, J. Phys. Chem. Solids 52 (1991) 537–544.
[65] J. Twu, C.J. Chuang, K.I. Chang, C.H. Yang, K.H. Chen, Raman spectroscopic studies on the sulfation of cerium oxide, Appl. Catalysis B: Environmental 12 (1997) 309–324.
[66] D.A. McKeown, I.S. Muller, H. Gan, Z. Feng, C. Viragh, I.L. Pegg, Vanadium and chromium redox behavior in borosilicate nuclear waste glasses, J. Non-Cryst. Solids 357 (2011) 2735–2743.
[67] W.D. Johnston, Optical spectra of the various valence states of vanadium in $Na_2O•2SiO_2$ glass, J. Am. Ceram. Soc. 48 (1965) 608–611.
[68] H. Farah, M. Brungs, Oxidation-reduction equilibria of vanadium in CaO-SiO_2, CaO-Al_2O_3-SiO_2 and CaO-MgO-SiO_2 melts, J. Mater. Sci. 38 (2003) 1885–1894.
[69] H. Farah, Optical basicity analysis of vanadium-bearing silicate glasses/melts, J. Am. Ceram. Soc. 91 (2008) 3915–3919.
[70] M. Leister, D. Ehrt, The influence of high melting temperatures on the behaviour of polyvalent ions in silicate glasses, Glasstech. Berl. Glass Sci. Technol. 73 C2 (2000) 194–203.
[71] W. Kauzmann, The nature of the glassy state and the behavior of liquids at low temperatures, Chem. Rev. 43 (1948) 219–256.
[72] M. Suzuki, N. Umeşaki, T. Tanaka, T. Ohkubo, T. Kakihara, T. Hashimoto, H. Kawashima, Structural behaviour of vanadium ions in alkali borosilicate glass for nuclear waste storage, Phys. Chem. Glasses 59 (2018) 181–192.
[73] O. Attos, M. Massot, M. Balkanski, E. Haro-Poniatowski, M. Asomoza, Structure of borovandate glasses studied by Raman spectroscopy, J. Non-Cryst. Solids 210 (1997) 163–170.
[74] G. Giuli, E. Paris, J. Mungall, C. Romano, D. Dingwell, V oxidation state and coordination number in silicate glasses by XAS, Am. Mineral. 89 (2004) 1640–1646.
[75] E.V. Galuskin, F. Gfeller, I.O. Galuskina, A. Pakhomova, T. Armbruster, Y. Vapnik, R. Włodyka, P. Dzierżanowski, M. Murashko, New minerals with a modular structure derived from hatrurite from the pyrometamorphic Hatrurim Complex. Part II. Zadovite, $BaCa_6[(SiO_4)(PO_4)](PO_4)_2F$ and aradite, $BaCa_6[(SiO_4)(VO_4)](VO_4)_2F$, from paralavas of the Hatrurim Basin, Negev Desert, Israel, Mineral. Mag 79 (2015) 1073–1087.
[76] I. Kansal, D.U. Tulyaganov, A. Goel, M.J. Pascual, J.M.F. Ferreira, Structural analysis and thermal behavior of diopside-fluorapatite-wollastonite-based glasses and glass-ceramics, Acta Biomater 6 (2010) 4380–4388.
[77] S. Hayakawa, T. Yoko, S. Sakka, Structural studies on alkaline earth vanadate glasses (Part 1) IR Spectroscopic Study, J. Ceram. Soc. Japan 102 (1994) 522–529.
[78] P. Liu, K. Januchta, L.R. Jensen, M. Bauchy, M.M. Smedskjaer, Competitive effects of free volume, rigidity, and self-adaptivity on indentation response of silicoaluminoborate glasses, J. Am. Ceram. Soc. 103 (2020) 944–954.
[79] K. Januchta, R.E. Youngman, A. Goel, M. Bauchy, S.L. Logunov, S.J. Rzoska, M. Bockowski, L.R. Jensen, M.M. Smedskjaer, Discovery of ultra-crack-resistant oxide glasses with adaptive networks, Chem. Mater. 29 (2017) 5865–5876.
[80] D.A. McKeown, H. Gan, I.L. Pegg, X-ray absorption and Raman spectroscopy studies of molybdenum environments in borosilicate waste glasses, J. Nucl. Mater. 488 (2017) 143–149.